Indian Journal of Pure & Applied Physics
Vol. 40, May 2002, pp. 342-349

Analytical two-dimensional model for pulsed doped InP-based lattice-matched HEMTs for high frequency applications

Ritesh Gupta, Mridula Gupta & R S Gupta

Semiconductor Device Research Laboratory, Department of Electronic Science,

University of Delhi, South Campus, New Delhi 110 021

(E-mail: rsgu@bol.net.in)

Received 29 August 2001; accepted 8 February 2002

An analytical two-dimensional model for pulsed doped HEMT is developed for InAlAs/InGaAs heterostructure using Greens function. Non-linear variation of sheet carrier density with quasi-Fermi energy is used to formulate the characteristics. The exact variation of sheet carrier density with gate voltage and the extension of gate boundaries with the variation of gate-to-drain and gate-to-source voltages are included in the analysis and the electric field profile has also been extensively studied considering the short channel effects. Results so obtained are in close proximity with published data.

1 Introduction

The conduction band discontinuity[1] between InAlAs and InGaAs is responsible for providing the necessary high sheet carrier density of 2D-electron gas within the InGaAs quantum well. The use of InGaAs material as a channel material having a large Γ-L valley separation[2] leads to higher carrier mobility and higher carrier saturation velocity. Ever since their development, significant efforts have been made to improve its speed and to optimize and predict the device performance[3-5]. The device length has been shrunk from 0.33 μm to 0.05 μm, thereby increasing the speed[6-15] from 50 GHz to over 250 GHz; but short gate length devices (≤ 0.6 μm) suffers from a high output conductance (g_o), which leads to reduction of the voltage gain (g_m/g_o) and breakdown voltage, thereby excluding them from power applications. In addition to kink effect[16-20] shortening the gate length also leads to short channel effects, which causes the channel charge and current to be partially controlled by the drain potential rather than the gate bias. Even if present to a small extent, short channel effects degrade the circuit performance by degrading the output conductance and consequently the gain. If present to a greater extent, it creates threshold voltage control problems. The gradual channel approximation (GCA) fails to include this effect as it ignores the effect of horizontal electric field penetrating from the source to drain. In order to account for DIBL effect the two-dimensional electric field distribution needs to be accurately predicted by solving two-dimensional Poisson's equation.

In the present analysis, two-dimensional Poisson's equation is solved using Green's function technique. The model is then extended to predict I_d-V_d characteristics and conductances. The variations of channel potential, electric field and sheet carrier density along the channel have also been investigated in details to give a clear insight into device physics. Close proximity with published results confirms the validity of the present approach.

2 Model Formulation

The cross-sectional view of InAlAs/InGaAs heterostructure is shown in Fig.1(a). Poisson's equation is solved for the two-dimensional potential distribution in the completely depleted InAlAs layer under the gate for a rectangular coordinate system shown in Fig. 1(b) and can be written as:

$$\frac{\partial^2\psi}{\partial x^2}+\frac{\partial^2\psi}{\partial y^2}=\begin{cases}0 & \text{for } 0\le y\le d_s\\ \dfrac{-qN_D}{\varepsilon} & \text{for } d_s\le y\le d_s+d_a\\ 0 & \text{for } d_s+d_a\le y\le d\end{cases} \quad \ldots(1)$$

under the following boundary conditions, given as

$$\psi(x',d)=\begin{cases}\dfrac{-qN_D}{2\varepsilon}x^2+V_s & \text{for } 0\le x\le L_s\\ V_g-\phi_m-\delta & \text{for } L_s\le x\le L_s+L_g\\ \dfrac{-qN_D}{2\varepsilon}(x-L_T)^2+V_d & \text{for } L_s+L_g\le x\le L_T\end{cases} \quad \ldots(2a)$$

$$\psi(0,y')=V_s \quad \ldots(2b)$$

$$\psi(L_T,y')=V_d \quad \ldots(2c)$$

$$\frac{\partial\psi(x,0)}{\partial y}=\frac{qn_s(x)}{\varepsilon} \quad \ldots(2d)$$

where N_D is the donor concentration in InAlAs layer, q is the electron charge, ε is the dielectric permittivity of InAlAs, L_T (= L_s + L_g + L_d) is the effective gate length, in which L_g is the gate length and L_s (L_d) is the extension of the gate boundaries towards source (drain) end and is given by:

and $L_d=\sqrt{\dfrac{2\varepsilon}{qN_D}(\phi_m-V_g-\delta+V_d)}$

Using Green's theorem[21], the potential distribution can be expressed as:

$$\psi(x,y)=\iint_s\frac{qN_D}{\varepsilon}G(x,y,x',y')dx'dy'-\int_c\psi(x',y')\frac{\partial G}{\partial n'}dS'+\int_c\frac{\partial\psi(x',y')}{\partial n'}G(x,y,x',y')dS' \quad \ldots(3)$$

where Green's function must satisfies the equation:

$$\nabla^2G(x,y,x',y')=-\delta(x-x')(y-y') \quad \ldots(4)$$

Green's function $G(x, y, x', y')$ for a rectangular system is obtained by solving Eq.(4) in which it is zero for the Drichlet's boundary condition at x =0, x = L_T and y = d and its normal component is zero for the Newman's boundary condition at y = 0 and is obtained as:

$$G(x,y,x',y')=\frac{2}{L_T}\sum_{m=1}^{\infty}\sin\ (k_mx)\sin\ (k_mx')A(y,y',k_m) \quad \ldots(5a)$$

$G(x, y, x', y')=$

$$\frac{2}{d}\sum_{n=1}^{\infty}\sin\ [k_n(y-d)]\sin\ [k_n(y'-d)]B(x,x',k_m) \quad \ldots(5b)$$

where $A(y, y', k_m)$ and $B(y, y', k_m)$ are:

$$A(y,y',k_m)=\begin{cases}\dfrac{\cosh\ (k_my)\sinh\ [k_m(d-y')]}{k_m\cosh\ (k_md)} & \text{for } y<y'\\ \dfrac{\cosh\ (k_my')\sinh\ [k_m(d-y)]}{k_m\cosh\ (k_md)} & \text{for } y>y'\end{cases} \quad \ldots(5c)$$

$$B(y,y',k_m)=\begin{cases}\dfrac{\sinh\ (k_nx)\sinh\ [k_n(L_T-x')]}{k_n\sinh\ (k_nL_T)} & \text{for } x<x'\\ \dfrac{\sinh\ (k_nx')\sinh\ [k_m(L_T-x)]}{k_n\sinh\ (k_nL_T)} & \text{for } x>x'\end{cases} \quad \ldots(5d)$$

$k_m=\dfrac{m\pi}{L_T}$, $k_n=\left(n-\dfrac{1}{2}\right)\dfrac{\pi}{d}$, m and n are integers and are greater than zero.

Substituting Eq. (5) into Eq. (3) and solving, one can obtain:

$\psi(x,y)=$

$$\frac{2}{L_T}\sum_{m=1}^{\infty}\frac{qN_D}{\varepsilon}\sin\ (k_mx)\left(\frac{1-(-1)^m}{k_m}\right)\int_0^d A(y';y,k_m)dy'$$

$$+\frac{2}{L_T}\sum_{m=1}^{\infty}\frac{\sin\ (k_mx)\cosh\ (k_my)}{\cosh\ (k_md)}\int_0^{L_T}\psi(x',d)\sin\ (k_mx')dx'$$

$$-\frac{2}{L_T}\sum_{m=1}^{\infty}\frac{\sin\ (k_mx)\sinh\ [k_m(d-y)]}{k_m\cosh\ (k_md)}\int_0^{L_T}\frac{\partial\psi(x',d)}{\partial y'}\sin\ (k_mx')dx'$$

$$+\frac{2}{d}\sum_{n=1}^{\infty}\frac{\sin\ [k_n(y-d)]\sinh\ [k_n(L_T-x)]}{\sinh\ (k_nL_T)}\int_0^d\psi(0,y')\sin\ [k_n(y'-d)]dy'$$

$$+\frac{2}{d}\sum_{n=1}^{\infty}\frac{\sin\ [k_n(y-d)]\sinh\ (k_n x)}{\sinh\ (k_n L_T)}$$

$$\int_0^d \psi(L_T, y')\sin\ [k_n(y'-d)]dy'$$

. . . ...(6)

where $\psi(x',y')$ and $\frac{\partial\psi(x',y')}{\partial y'}$ represent the potential and normal electric field at the boundaries. The values of integrals obtained, in Eq. (6) and are given in the appendix.

I_d-V_d Model

The channel current (I_d) can be obtained from quasi-Fermi energy E_f as[22]:

$$I_d=-W\mu\, n_s(x)\frac{dE_f}{dx} \qquad ...(7)$$

where W is the gate width, μ is the field-dependent mobility and is given by:

$$\mu=\mu_0\left(\frac{1}{1+(E_{vp}/E_{vr})^{\beta}}\right)^{1/\beta} \qquad ...(8)$$

where β is ranging from 1 to 2.

$E_{vp}=\frac{dV_c}{dx}-\left(\frac{dV_c}{dx}\right)_{V_d=0}$ and $E_{vr}=\frac{V_{sat}}{\mu_0}$, in which $\frac{dV_c}{dx}$ denotes the electric field along the channel.

Integration of Eq. (7) from source to some point x in the channel results in:

$$-\left(\frac{E_f(x)-E_f(s)}{q}\right)=I_d R_s+\frac{I_d}{qW}\int_0^x\frac{dx}{\mu n_s} \qquad ...(9)$$

where R_s is the resistance between source and gate. $E_f(x)$ and $E_f(s)$ are the position of fermi level at some point x in the channel and at source end respectively.

The relation between quasi-Fermi level and channel potential for a HEMT is given as:

$$-\frac{E_f(x)-E_f(s)}{q}=V_c(x)+\frac{\Delta E_c}{q}-\delta-\frac{E_{fi}}{q} \qquad ...(10)$$

where ΔE_c is the conduction band discontinuity, E_{fi} is the position of Fermi level with respect to the bottom of the conduction band in InGaAs, $V_c(x)$ is the channel potential and can be calculated by substituting $y = 0$ in Eq.(6).

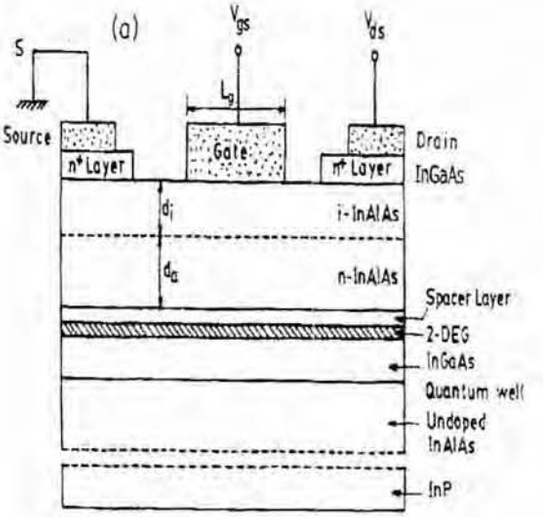

Fig. 1(a) — Schematic cross-section of a recessed-gate HEMT showing approximate extension of a depleted region (shaded region)

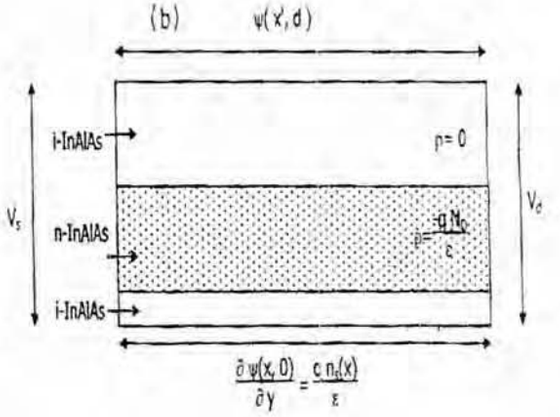

Fig. 1(b) — Boundary conditions for the depleted InAlAs region under the gate

Comparing Eqs (9) and (10), one can get:

$$V_c(x)+\frac{\Delta E_c}{q}-\delta-\frac{E_{fi}}{q}=I_d R_s+\frac{I_d}{qW}\int_0^x\frac{dx}{\mu n_s} \qquad ...(11)$$

The drain current for InAlAs/InGaAs/InP HEMT can also be obtained from:

$$I_d = \frac{V_d - V_s}{R} \qquad \ldots(12)$$

where V_d–V_s is the potential difference between source and drain and R is the equivalent resistance across drain-to-source and is given by:

$$R = R_s + R_d + \frac{1}{qW}\int_0^{L_g} \frac{dx}{\mu n_s} \qquad \ldots(13)$$

Eliminating I_d from Eqs (11) and (12) one can get:

$$\left(V_c(x) + \frac{\Delta E_c}{q} - \delta\right) - \frac{E_{fi}}{q} = \frac{(V_d - V_s)\left(R_s + \frac{1}{qW}\int_0^{x} \frac{dx}{\mu n_s}\right)}{R_s + R_d + \frac{1}{qW}\int_0^{L_g} \frac{dx}{\mu n_s}} \qquad \ldots(14)$$

which is the required integral equation for n_s.

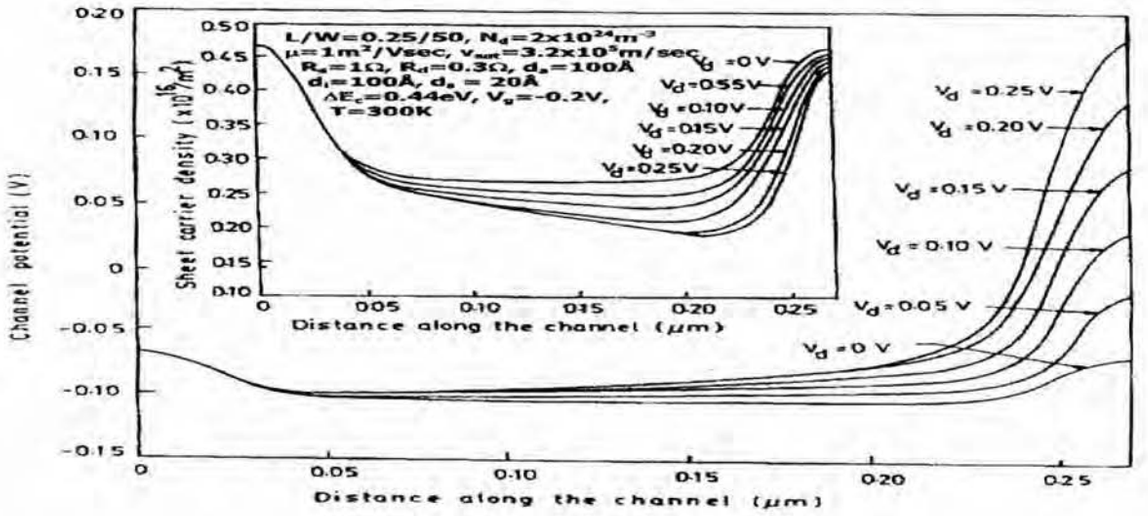

Fig. 2 — Channel potential along the channel for V_g = -0.2 and for V_d varying from 0 to 0.25 V in steps of 0.05 V. Inset shows 2-DEG sheet carrier density along the channel corresponding to V_g = -0.2 V for V_d varying from 0 to 0.25 V in steps of 0.05 V

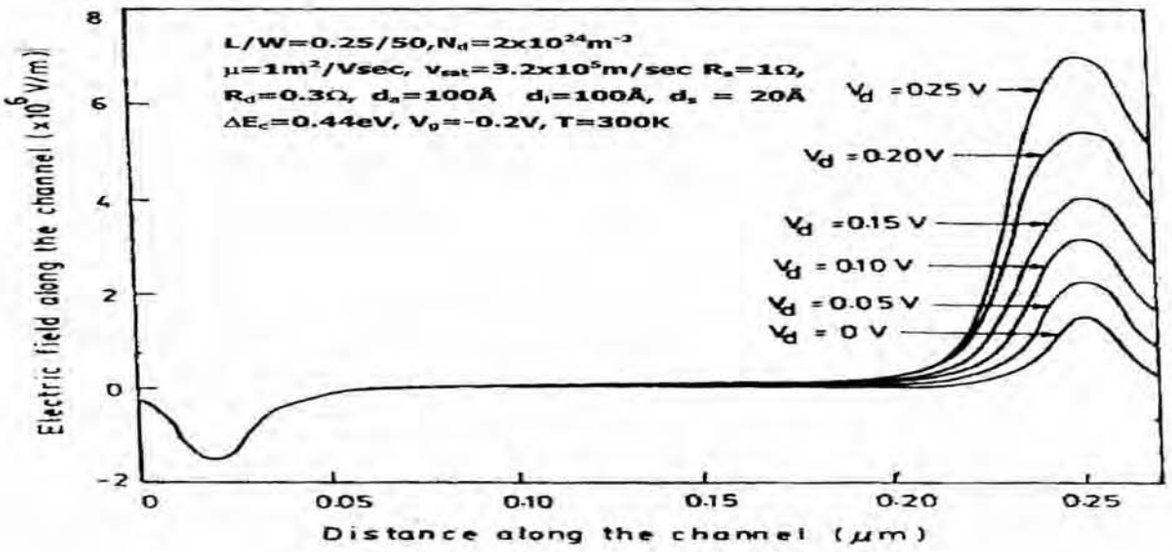

Fig. 3 — Electric field component along the channel corresponding to V_g= -0.2 V for V_d carrying from 0 to 0.25 V in steps of 0.05 V

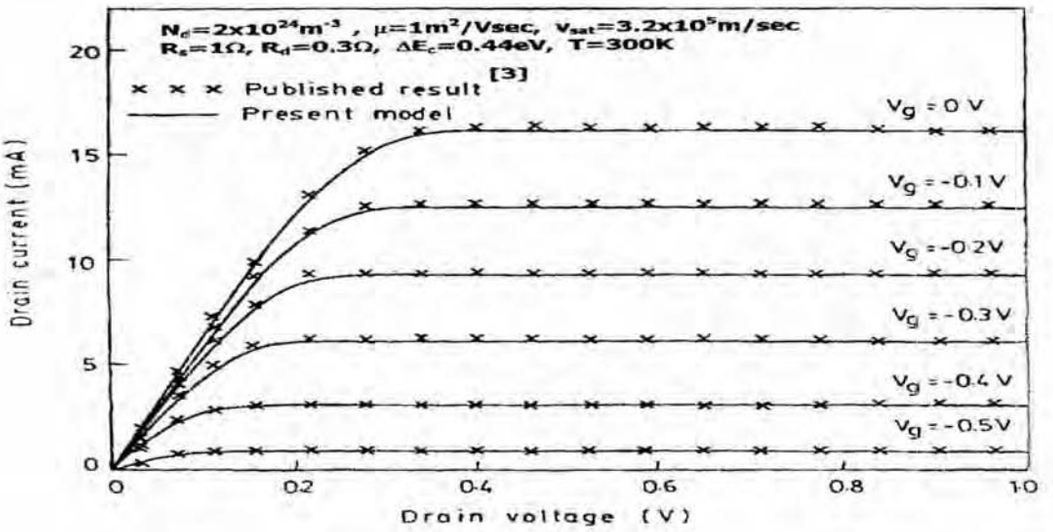

Fig. 4 — Variation of drain current with drain voltage for the assumed 0.25 μm gate length MODFET structure

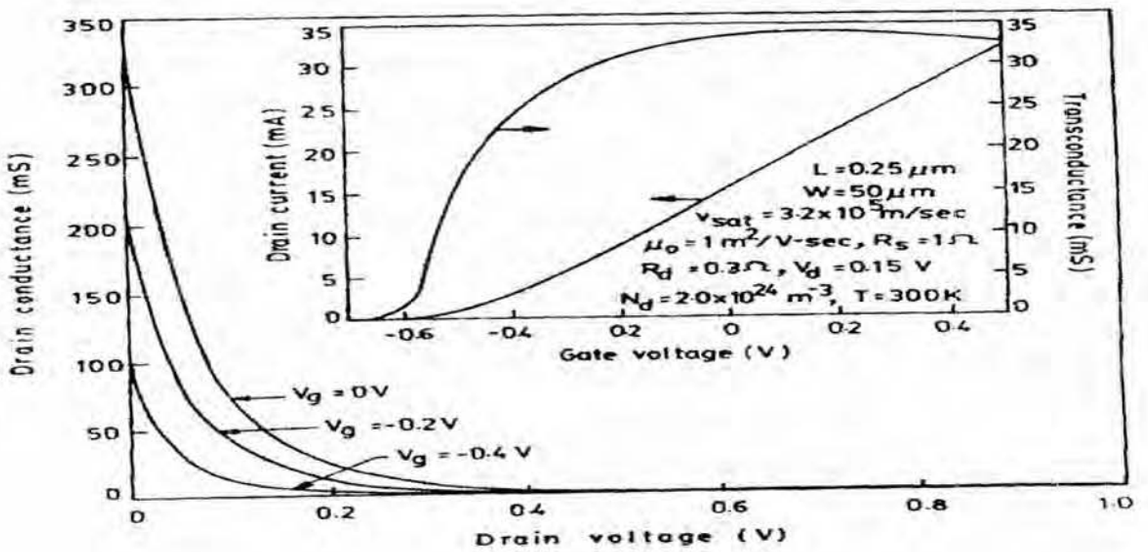

Fig. 5 — Variation of drain current and trans-conductance with gate voltage for 0.25 μm gate length MODFET structure (Inset shows the variation of drain-conductance with drain voltage for 0.25 μm gate length MODFET structure)

In order to solve Eq.(14) the authors used the simplified expression relating 2-DEG concentration with quasi-Fermi level reported in their earlier paper[23], and is given as:

$$\frac{E_{fi}}{q} = k_1 + k_2 n_s^{1/2} + k_3 n_s \qquad \ldots(15)$$

where k_1, k_2 and k_3 are constants.

Substituting Eq.(15) in Eq.(14) and assuming $V_0 = V_s = 0$, one can get:

$$\left(V_i(x) + \frac{\Delta E_c}{q} - \delta\right) - (k_1 + k_2 n_s^{1/2} + k_3 n_s) = 0 \qquad \ldots(16)$$

The above equation is a simple non-linear Volterra integral equation and can be easily solved for n_s. But for other values of V_d, Eq. (14) becomes too, complicated and thus solution is obtained by Newton-Raphson's method considering the solution of above equation as initial guess. Once the correct expression for 2-DEG sheet carrier density is obtained, channel potential, electric field and I_d-V_d characteristics can be found.

Trans-conductance and drain-conductance are obtained using drain current expression (12) and are expressed as:

$$g_m = \frac{\partial I_d}{\partial V_g}\Big|_{V_d} \qquad \ldots(17)$$

and

$$g_d = \frac{\partial I_d}{\partial V_d}\Big|_{V_g} \qquad \ldots(18)$$

Cut-off frequency of InAlAs/InGaAs/InP HEMT can be calculated as:

$$f_t = \frac{g_m}{2\pi C_g} \qquad \ldots(19)$$

where C_g is the gate capacitance.

3 Results and Discussion

Fig. 2 shows the variation of channel potential along the channel length for different drain voltages ranging from $V_d = 0$ V to $V_d = 0.25$ V. The variation of potential distribution with drain voltage at a constant gate bias indicates the drain-induced barrier lowering (DIBL) effect. From the figure it is also evident that the channel potential at the source end increases slightly and is due to the extension of depletion width below n^+ region. Inset of Fig. 2 shows the variation of 2-DEG concentration along the channel length with variation of drain voltage ranging from $V_d = 0$ V to $V_d = 0.25$ V. It can be seen from the figure that after saturation, sheet carrier density increases rapidly in the region nearer to the drain. Thus, most of the applied drain voltage appears across this narrow region of small conductance, which leads to larger electric field and can also be seen in Fig. 3. This sudden increase in electric field in this region makes the electron drift velocity to reach its scattering limiting value (3.2×10^5 m/sec).

Fig. 3 shows the variation of electric field along the channel. Towards the source end electric field is negative and increases gradually under the gate and then becomes significant in the region nearer to the drain, reaches it's maximum and then decreases. This decrease is due to change in channel potential towards the drain end. The electric field shows a large variation towards the drain end thus showing the importance of solving two-dimensional Poisson's equation in the saturation region.

Fig. 4 shows the variation of drain current with drain voltage with gate voltage as parameter. Results have been plotted for gate voltage ranging from 0 to -0.5 V and have been compared with the model proposed by Chen *et al.*[3] Close proximity with published results shows the validity of our model.

Variations of drain current and trans-conductance with gate voltage at a constant drain voltage are shown in Fig. 5. For a set of parameters, the threshold voltage obtained from the graph is –0.5 V. The maximum value of trans-conductance is 33 mS at 0.1 V of the applied gate voltage. The cut-off frequency is found to be 84 GHz, which makes InAlAs/InGaAs/InP HEMT suitable for microwave frequency applications. Inset of Fig. 5 shows the dependence of output conductance on drain voltages for various gate biases. Drain conductance falls appreciably as drain bias is increased and finally approaches zero as the applied drain bias is increased further. It can be seen from the graph that as the applied gate bias is increased, the saturation drain conductance increases.

4 Conclusion

A two-dimensional charge-control model for 2-D potential distribution, sheet carrier density and electric field distribution of a short-channel InAlAs/InGaAs/InP MODFET has been developed using Green's function approach. Further the model has been extended to calculate trans-conductance and drain conductance. Thus, the model provides clear insight of current saturation that considers channel potential, 2-DEG sheet carrier concentration and electric field characteristics.

Acknowledgement

The authors are thankful to Defence Research Development Organization, Ministry of Defence,

Government of India, for providing the necessary financial assistance.

References

1 Weslch D F, Wicks G W & Eastman L F, *J Appl Phys*, 55 (1984) 3176.

2 Chen K Y, Cho A Y, Christman S G, Pearsall T P & Rowe J E, *Appl Phys Lett*, 40 (1980) 423.

3 Chen J W, Thurairaj M & Das M B, *IEEE Trans Electron Devices*, 41 (1994) 465.

4 Guan Lee, Christou Aris, Halkias George & Barbe D F, *IEEE Trans Electron Devices*, 42 (1995) 612.

5 Mitra H, Pal B B, Singh S & Khan R U, *IEEE Trans Electron Devices*, 45 (1998) 68.

6 Camnitz L H, Tasker P J, Lee H, Van der Merwe D & Eastman L F, in *IEDM Tech Dig*, 360.

7 Lepore N, Levy M, Tiberio R, Tasker P, Lee H, Wolf E, Eastman L & Kphn E, *Electron Lett*, 24 (1988) 364.

8 Moll N, Hueschen M R & Fischer-Colbrie A, *IEEE Trans Electron Devices*, 35 (1988) 878.

9 Nguyen L D, Tasker P J, Radulescu D C & Eastman L F, *IEEE Trans Electron Devices*, 36 (1989) 2243.

10 Mishra U K, Brown A S & Rosenbaum S E, in *IEDM Tech Dig*, (1988) 180.

11 Mishra U K, Brown A S, Jelloian L M, Thompson M, Nguyen L D & Rosenbaum S E, in *IEDM Tech Dig*, (1989) 101.

12 Nguyen L D, Jelloian L M, Thompson M A & Lui M, in *IEDM Tech Dig*, (1990) 101.

13 Nguyen L D, Brown A S, Thompson M A & Jelloian L M, *IEEE Trans Electon Devices*, 39 (1992) 2007.

14 Smith P M, Jiu S M J, Kao M Y, Ho P, Wang S C, Duh K H G, Fu S T & Chao P C, *IEEE Microwave and Guided Wave Lett*, 5 (1995) 230.

15 Enoki T, Yokoyama H, Umeda Y & Otsuji T, *Jpn J Appl Phys*, 37 (1998) 1359.

16 Brown S, Mishra U K, Chou C S, Hooper C E, Melendes M A, Thompson M, Larson L E, Rosenbaum S E & Deleney M J, *IEEE EDL*, 10 (1989) 565.

17 Pao Y C, Nishimoto C K, Majidi R A, Archer J, Bechtel N G & Harris J S, *IEEE Trans Electron Devices*, 37 (1990) 2165.

18 Mishra U K, *et al.*: Int Symp on GaAs and related compounds, *Tech Dig*, (1991) 344.

19 Pao Y C *et al.*; Third Int Conf on InP and related materials, *Tech Dig*, (1991) 344.

20 Zhou G G, Colbrie A F, Miller J, Pao Y C, Hughes B, Studebaker L & Harris J S, in *IEDM Tech Dig*, (1991) 247.

21 Jackson J D, *Classical electrodynamics*, (Wiley, New York), 1975.

22 Arora N, *MOSFET models for VLSI circuit simulation*, (Springer-Verlag, Wien), 1993.

23 Gupta R, Kranti A, Haldar S, Gupta M & Gupta R S, *Microelectronic engineering*, (2001) (in press).

Appendix

(A)

$$\int_0^d A(y';y,k_m)\,dy' =$$

$$\frac{\cosh(k_m y)}{k_m \cosh(k_m d)}\left(\frac{\cosh[k_m(d-d_s)]-\cosh(k_m d_i)}{k_m}\right)$$

for $y < d_s$

$$\int_0^d A(y';y,k_m)\,dy' =$$

$$\frac{\sinh[k_m(d-y)]}{k_m \cosh(k_m d)}\left(\frac{\sinh(k_m y)-\sinh(k_m d_s)}{k_m}\right)$$

$$+\frac{\cosh(k_m y)}{k_m \cosh(k_m d)}\left(\frac{\cosh[k_m(d-y)]-\cosh(k_m d_i)}{k_m}\right)$$

for $d_s < y < d_s + d_a$

$$\int_0^d A(y';y,k_m)\,dy' =$$

$$\frac{\sinh[k_m(d-y)]}{k_m \cosh(k_m d)}\left(\frac{\sinh[k_m d_s + d_a)]-\sinh(k_m d_s)}{k_m}\right)$$

otherwise

(B)

$$\int_0^{L_g} \psi(x',d)\sin(k_m x')dx' = A_1 + A_2 + A_3 + A_4$$

$$A_1 = \frac{qN_D L_s^2}{2\varepsilon k_m}\left(\cos(k_m L_s) - \frac{2\sin(k_m L_s)}{L_s k_m}\right)$$

$$A_2 = \frac{-qN_D}{\varepsilon}\left(\frac{\cos(k_m L_s)-1}{k_m^3}\right)$$

$$-(V_g - \phi_m - \delta)\left(\frac{\cos[k_m(L_g+L_s)]-\cos(k_m L_s)}{k_m}\right)$$

$$A_3 = V_d\left(\frac{\cos(k_m[L_g + L_s)] - (-1)^m}{k_m}\right)$$

$$-\frac{qN_D L_d^2}{2\varepsilon}\left(\frac{\cos\,[k_m(L_g + L_s)]}{k_m}\right)$$

$$A_4 = \frac{-qN_D L_d}{\varepsilon k_m^2}$$

$$\left(\sin[k_m(L_g + L_s)] - \left(\frac{\cos[k_m(L_g + L_s)] - (-1)^m}{k_m}\right)\right)$$

(C)

$$\int_0^d \psi(0, y')\sin[k_n(y' - d)]dy' = \frac{-V_s}{k_n}$$

(D)

$$\int_0^d \psi(L_T, y')\sin[k_n(y' - d)]dy' = \frac{-V_d}{k_n}$$